Title

J/psi polarization in p plus p collisions at root s=200 GeV in STAR

Authors

Adamczyk, L
Adkins, JK
Agakishiev, G
et al.

Publication Date

2014-12-12

DOI

10.1016/j.physletb.2014.10.049

J/ψ polarization in $p+p$ collisions at $\sqrt{s} = 200$ GeV in STAR

L. Adamczyk,[1] J. K. Adkins,[23] G. Agakishiev,[21] M. M. Aggarwal,[35] Z. Ahammed,[54] I. Alekseev,[19] J. Alford,[22] C. D. Anson,[32] A. Aparin,[21] D. Arkhipkin,[4] E. C. Aschenauer,[4] G. S. Averichev,[21] J. Balewski,[27] A. Banerjee,[54] Z. Barnovska,[14] D. R. Beavis,[4] R. Bellwied,[50] A. Bhasin,[20] A. K. Bhati,[35] P. Bhattarai,[49] H. Bichsel,[56] J. Bielcik,[13] J. Bielcikova,[14] L. C. Bland,[4] I. G. Bordyuzhin,[19] W. Borowski,[46] J. Bouchet,[22] A. V. Brandin,[30] S. G. Brovko,[6] S. Bültmann,[33] I. Bunzarov,[21] T. P. Burton,[4] J. Butterworth,[41] H. Caines,[57] M. Calderón de la Barca Sánchez,[6] D. Cebra,[6] R. Cendejas,[36] M. C. Cervantes,[48] P. Chaloupka,[13] Z. Chang,[48] S. Chattopadhyay,[54] H. F. Chen,[43] J. H. Chen,[45] L. Chen,[9] J. Cheng,[51] M. Cherney,[12] A. Chikanian,[57] W. Christie,[4] J. Chwastowski,[11] M. J. M. Codrington,[49] R. Corliss,[27] J. G. Cramer,[56] H. J. Crawford,[5] X. Cui,[43] S. Das,[16] A. Davila Leyva,[49] L. C. De Silva,[50] R. R. Debbe,[4] T. G. Dedovich,[21] J. Deng,[44] A. A. Derevschikov,[37] R. Derradi de Souza,[8] S. Dhamija,[18] B. di Ruzza,[4] L. Didenko,[4] C. Dilks,[36] F. Ding,[6] P. Djawotho,[48] X. Dong,[26] J. L. Drachenberg,[53] J. E. Draper,[6] C. M. Du,[25] L. E. Dunkelberger,[7] J. C. Dunlop,[4] L. G. Efimov,[21] J. Engelage,[5] K. S. Engle,[52] G. Eppley,[41] L. Eun,[26] O. Evdokimov,[10] R. Fatemi,[23] S. Fazio,[4] J. Fedorisin,[21] P. Filip,[21] E. Finch,[57] Y. Fisyak,[4] C. E. Flores,[6] C. A. Gagliardi,[48] D. R. Gangadharan,[32] D. Garand,[38] F. Geurts,[41] A. Gibson,[53] M. Girard,[55] S. Gliske,[2] D. Grosnick,[53] Y. Guo,[43] A. Gupta,[20] S. Gupta,[20] W. Guryn,[4] B. Haag,[6] O. Hajkova,[13] A. Hamed,[48] L-X. Han,[45] R. Haque,[31] J. W. Harris,[57] J. P. Hays-Wehle,[27] S. Heppelmann,[36] A. Hirsch,[38] G. W. Hoffmann,[49] D. J. Hofman,[10] S. Horvat,[57] B. Huang,[4] H. Z. Huang,[7] X. Huang,[51] P. Huck,[9] T. J. Humanic,[32] G. Igo,[7] W. W. Jacobs,[18] H. Jang,[24] E. G. Judd,[5] S. Kabana,[46] D. Kalinkin,[19] K. Kang,[51] K. Kauder,[10] H. W. Ke,[4] D. Keane,[22] A. Kechechyan,[21] A. Kesich,[6] Z. H. Khan,[10] D. P. Kikola,[55] I. Kisel,[15] A. Kisiel,[55] D. D. Koetke,[53] T. Kollegger,[15] J. Konzer,[38] I. Koralt,[33] W. Korsch,[23] L. Kotchenda,[30] P. Kravtsov,[30] K. Krueger,[2] I. Kulakov,[15] L. Kumar,[31] R. A. Kycia,[11] M. A. C. Lamont,[4] J. M. Landgraf,[4] K. D. Landry,[7] J. Lauret,[4] A. Lebedev,[4] R. Lednicky,[21] J. H. Lee,[4] W. Leight,[27] M. J. LeVine,[4] C. Li,[43] W. Li,[45] X. Li,[38] X. Li,[47] Y. Li,[51] Z. M. Li,[9] L. M. Lima,[42] M. A. Lisa,[32] F. Liu,[9] T. Ljubicic,[4] W. J. Llope,[41] R. S. Longacre,[4] X. Luo,[9] G. L. Ma,[45] Y. G. Ma,[45] D. M. M. D. Madagodagettige Don,[12] D. P. Mahapatra,[16] R. Majka,[57] S. Margetis,[22] C. Markert,[49] H. Masui,[26] H. S. Matis,[26] D. McDonald,[50] T. S. McShane,[12] N. G. Minaev,[37] S. Mioduszewski,[48] B. Mohanty,[31] M. M. Mondal,[48] D. A. Morozov,[37] M. G. Munhoz,[42] M. K. Mustafa,[26] B. K. Nandi,[17] Md. Nasim,[31] T. K. Nayak,[54] J. M. Nelson,[3] L. V. Nogach,[37] S. Y. Noh,[24] J. Novak,[29] S. B. Nurushev,[37] G. Odyniec,[26] A. Ogawa,[4] K. Oh,[39] A. Ohlson,[57] V. Okorokov,[30] E. W. Oldag,[49] R. A. N. Oliveira,[42] M. Pachr,[13] B. S. Page,[18] S. K. Pal,[54] Y. X. Pan,[7] Y. Pandit,[10] Y. Panebratsev,[21] T. Pawlak,[55] B. Pawlik,[34] H. Pei,[9] C. Perkins,[5] W. Peryt,[55] P. Pile,[4] M. Planinic,[58] J. Pluta,[55] D. Plyku,[33] N. Poljak,[58] J. Porter,[26] A. M. Poskanzer,[26] N. K. Pruthi,[35] M. Przybycien,[1] P. R. Pujahari,[17] H. Qiu,[26] A. Quintero,[22] S. Ramachandran,[23] R. Raniwala,[40] S. Raniwala,[40] R. L. Ray,[49] C. K. Riley,[57] H. G. Ritter,[26] J. B. Roberts,[41] O. V. Rogachevskiy,[21] J. L. Romero,[6] J. F. Ross,[12] A. Roy,[54] L. Ruan,[4] J. Rusnak,[14] N. R. Sahoo,[54] P. K. Sahu,[16] I. Sakrejda,[26] S. Salur,[26] A. Sandacz,[55] J. Sandweiss,[57] E. Sangaline,[6] A. Sarkar,[17] J. Schambach,[49] R. P. Scharenberg,[38] A. M. Schmah,[26] W. B. Schmidke,[4] N. Schmitz,[28] J. Seger,[12] P. Seyboth,[28] N. Shah,[7] E. Shahaliev,[21] P. V. Shanmuganathan,[22] M. Shao,[43] B. Sharma,[35] W. Q. Shen,[45] S. S. Shi,[26] Q. Y. Shou,[45] E. P. Sichtermann,[26] R. N. Singaraju,[54] M. J. Skoby,[18] D. Smirnov,[4] N. Smirnov,[57] D. Solanki,[40] P. Sorensen,[4] U. G. deSouza,[42] H. M. Spinka,[2] B. Srivastava,[38] T. D. S. Stanislaus,[53] J. R. Stevens,[27] R. Stock,[15] M. Strikhanov,[30] B. Stringfellow,[38] A. A. P. Suaide,[42] M. Sumbera,[14] X. Sun,[26] X. M. Sun,[26] Y. Sun,[43] Z. Sun,[25] B. Surrow,[47] D. N. Svirida,[19] T. J. M. Symons,[26] A. Szanto de Toledo,[42] J. Takahashi,[8] A. H. Tang,[4] Z. Tang,[43] T. Tarnowsky,[29] J. H. Thomas,[26] A. R. Timmins,[50] D. Tlusty,[14] M. Tokarev,[21] S. Trentalange,[7] R. E. Tribble,[48] P. Tribedy,[54] B. A. Trzeciak,[55] O. D. Tsai,[7] J. Turnau,[34] T. Ullrich,[4] D. G. Underwood,[2] G. Van Buren,[4] G. van Nieuwenhuizen,[27] J. A. Vanfossen, Jr.,[22] R. Varma,[17] G. M. S. Vasconcelos,[8] A. N. Vasiliev,[37] R. Vertesi,[14] F. Videbæk,[4] Y. P. Viyogi,[54] S. Vokal,[21] A. Vossen,[18] M. Wada,[49] M. Walker,[27] F. Wang,[38] G. Wang,[7] H. Wang,[4] J. S. Wang,[25] X. L. Wang,[43] Y. Wang,[51] Y. Wang,[10] G. Webb,[23] J. C. Webb,[4] G. D. Westfall,[29] H. Wieman,[26] S. W. Wissink,[18] R. Witt,[52] Y. F. Wu,[9] Z. Xiao,[51] W. Xie,[38] K. Xin,[41] H. Xu,[25] N. Xu,[26] Q. H. Xu,[44] Y. Xu,[43] Z. Xu,[4] W. Yan,[51] C. Yang,[43] Y. Yang,[25] Y. Yang,[9] Z. Ye,[10] P. Yepes,[41] L. Yi,[38] K. Yip,[4] I-K. Yoo,[39] Y. Zawisza,[43] H. Zbroszczyk,[55] W. Zha,[43] J. B. Zhang,[9] J. L. Zhang,[44] S. Zhang,[45] X. P. Zhang,[51] Y. Zhang,[43] Z. P. Zhang,[43] F. Zhao,[7] J. Zhao,[9] C. Zhong,[45] X. Zhu,[51] Y. H. Zhu,[45] Y. Zoulkarneeva,[21] and M. Zyzak[15]

(STAR Collaboration)

[1] *AGH University of Science and Technology, Cracow, Poland*

[2]Argonne National Laboratory, Argonne, Illinois 60439, USA
[3]University of Birmingham, Birmingham, United Kingdom
[4]Brookhaven National Laboratory, Upton, New York 11973, USA
[5]University of California, Berkeley, California 94720, USA
[6]University of California, Davis, California 95616, USA
[7]University of California, Los Angeles, California 90095, USA
[8]Universidade Estadual de Campinas, Sao Paulo, Brazil
[9]Central China Normal University (HZNU), Wuhan 430079, China
[10]University of Illinois at Chicago, Chicago, Illinois 60607, USA
[11]Cracow University of Technology, Cracow, Poland
[12]Creighton University, Omaha, Nebraska 68178, USA
[13]Czech Technical University in Prague, FNSPE, Prague, 115 19, Czech Republic
[14]Nuclear Physics Institute AS CR, 250 68 Řež/Prague, Czech Republic
[15]Frankfurt Institute for Advanced Studies FIAS, Germany
[16]Institute of Physics, Bhubaneswar 751005, India
[17]Indian Institute of Technology, Mumbai, India
[18]Indiana University, Bloomington, Indiana 47408, USA
[19]Alikhanov Institute for Theoretical and Experimental Physics, Moscow, Russia
[20]University of Jammu, Jammu 180001, India
[21]Joint Institute for Nuclear Research, Dubna, 141 980, Russia
[22]Kent State University, Kent, Ohio 44242, USA
[23]University of Kentucky, Lexington, Kentucky, 40506-0055, USA
[24]Korea Institute of Science and Technology Information, Daejeon, Korea
[25]Institute of Modern Physics, Lanzhou, China
[26]Lawrence Berkeley National Laboratory, Berkeley, California 94720, USA
[27]Massachusetts Institute of Technology, Cambridge, MA 02139-4307, USA
[28]Max-Planck-Institut für Physik, Munich, Germany
[29]Michigan State University, East Lansing, Michigan 48824, USA
[30]Moscow Engineering Physics Institute, Moscow Russia
[31]National Institute of Science Education and Research, Bhubaneswar 751005, India
[32]Ohio State University, Columbus, Ohio 43210, USA
[33]Old Dominion University, Norfolk, VA, 23529, USA
[34]Institute of Nuclear Physics PAN, Cracow, Poland
[35]Panjab University, Chandigarh 160014, India
[36]Pennsylvania State University, University Park, Pennsylvania 16802, USA
[37]Institute of High Energy Physics, Protvino, Russia
[38]Purdue University, West Lafayette, Indiana 47907, USA
[39]Pusan National University, Pusan, Republic of Korea
[40]University of Rajasthan, Jaipur 302004, India
[41]Rice University, Houston, Texas 77251, USA
[42]Universidade de Sao Paulo, Sao Paulo, Brazil
[43]University of Science & Technology of China, Hefei 230026, China
[44]Shandong University, Jinan, Shandong 250100, China
[45]Shanghai Institute of Applied Physics, Shanghai 201800, China
[46]SUBATECH, Nantes, France
[47]Temple University, Philadelphia, Pennsylvania, 19122, USA
[48]Texas A&M University, College Station, Texas 77843, USA
[49]University of Texas, Austin, Texas 78712, USA
[50]University of Houston, Houston, TX, 77204, USA
[51]Tsinghua University, Beijing 100084, China
[52]United States Naval Academy, Annapolis, MD 21402, USA
[53]Valparaiso University, Valparaiso, Indiana 46383, USA
[54]Variable Energy Cyclotron Centre, Kolkata 700064, India
[55]Warsaw University of Technology, Warsaw, Poland
[56]University of Washington, Seattle, Washington 98195, USA
[57]Yale University, New Haven, Connecticut 06520, USA
[58]University of Zagreb, Zagreb, HR-10002, Croatia

We report on a polarization measurement of inclusive J/ψ mesons in the di-electron decay channel at mid-rapidity at $2 < p_T < 6$ GeV/c in $p+p$ collisions at $\sqrt{s} = 200$ GeV. Data were taken with the STAR detector at RHIC. The J/ψ polarization measurement should help to distinguish between different models of the J/ψ production mechanism since they predict different p_T dependences of the J/ψ polarization. In this analysis, J/ψ polarization is studied in the helicity frame. The polarization parameter λ_θ measured at RHIC becomes smaller towards high p_T, indicating more longitudinal

J/ψ polarization as p_T increases. The result is compared with predictions of presently available models.

PACS numbers: 25.75.Dw, 13.20.Gd, 14.40.Lb

I. INTRODUCTION

The J/ψ is a bound state of charm (c) and anti-charm ($\overline{c}$) quarks. Charmonia physical states have to be colorless, however they can be formed via a color-singlet or a color-octet intermediate $c\overline{c}$ state. The first model of charmonia production, the Color Singlet Model (CSM) [1–8], assumed that $c\overline{c}$ pairs are created in the color-singlet state only. This early prediction failed to describe the measured charmonia cross-section which has led to the development of new models. For example, Non-Relativistic QCD (NRQCD) [9] calculations were proposed in which a $c\overline{c}$ color-octet intermediate state, in addition to a color-singlet state, can bind to form a charmonium.

Different models of J/ψ production are able to describe the measured J/ψ production cross section reasonably well [10–17] and therefore other observables are needed to discriminate between different J/ψ production mechanisms. J/ψ spin alignment, commonly known as polarization, can be used for this purpose, since various models predict different transverse momentum (p_T) dependence for the polarization. The predictions of different models deviate the most at high p_T. Therefore a high-p_T J/ψ polarization measurement is of particular interest since it can help to discriminate between the models.

NRQCD calculations with color-octet contributions [18] are in good agreement with observed J/ψ p_T spectra in different experiments at different energies, at the Relativistic Heavy Ion Collider (RHIC) [11, 12], the Tevatron [13, 14] and the Large Hadron Collider (LHC) [16, 17, 19]. But the calculations fail to describe the J/ψ polarization at high p_T ($p_T > 5$ GeV/c) measured by the CDF experiment at FermiLab at $\sqrt{s} = 1.96$ TeV [20]. NRQCD calculations predict transverse polarization for $p_T > 5$ GeV/c and the growth of the polarization parameter λ_θ with increasing p_T [21]. However, the CDF polarization measurement becomes slightly longitudinal with increasing p_T, for $5 < p_T < 30$ GeV/c [20]. Also, the CMS J/ψ polarization measurement in $p+p$ collisions at $\sqrt{s}$ = 7 TeV for high transverse momenta [22] is in disagreement with existing next-to-leading-order (NLO) NRQCD calculations [21, 23]. In addition, the J/ψ polarization measurements at the same energy and for lower p_T were performed by ALICE (inclusive J/ψ production) [24] and LHCb (prompt J/ψ production) [25] experiments at forward rapidity. The ALICE experiment observed zero polarization while LHCb λ_θ results indicate small longitudinal polarization (with other coefficients consistent with zero). Data from both experiments favor NLO NRQCD over NLO CSM [21, 25]. At RHIC energies, at intermediate p_T ($1.5 < p_T \lesssim 5$ GeV/c) and for mid-rapidity, the tuned leading-order (LO) NRQCD model [26] predicts slightly longitudinal J/ψ polarization and describes the PHENIX result [27] well.

In the case of the Color Singlet Model, the Next-to-Leading Order calculations (NLO$^+$ CSM) [28] for the p_T spectrum are in near agreement with the RHIC data at low and mid p_T and these CSM calculations predict longitudinal J/ψ polarization at intermediate p_T ($1.5 < p_T < 6$ GeV/c) at mid-rapidity which is in agreement with the PHENIX result [28]. At the Tevatron and LHC energies, the upper bound of NNLO* prediction [29] is very close to the experimental cross section data, similar to RHIC [28]. Also, the upper edge of this prediction for the polarization is in good agreement with the CDF data [29]. However, NLO CSM calculations [21, 25] do not describe J/ψ polarization results from ALICE and LHCb well.

For the lower p_T range at RHIC energies, the LO NRQCD calculations [26] and NLO$^+$ CSM [28] have similar predictions regarding the J/ψ polarization, which is longitudinal, and describe the experimental results[27] well. However, these models predict different p_T dependence: in the case of the NRQCD prediction, the trend is towards the transverse polarization with increasing p_T, while the NLO$^+$ CSM shows almost no p_T dependence. Thus, it is especially important to measure a p_T dependence of the J/ψ polarization and go to high p_T.

In this paper, we report a J/ψ polarization measurement in $p+p$ collisions at $\sqrt{s} = 200$ GeV at rapidity (y) $|y| < 1$, in the p_T range $2 < p_T < 6$ GeV/c from the STAR experiment at RHIC. The analysis is done using data with a high-p_T electron (so-called High Tower) trigger. The J/ψ is reconstructed via its di-electron decay channel. The angular distribution parameter (polarization parameter) λ_θ for electron decay of the J/ψ is extracted in the helicity frame [30] as a function of J/ψ p_T, in three p_T bins. The obtained result is compared with predictions of NLO$^+$ CSM [28] and LO NRQCD calculations (COM) [26].

A. Angular distribution of decay products

J/ψ polarization is analyzed via the angular distribution of the decay electrons in the helicity frame [30]. In this analysis, we are interested in the polar angle θ. It is the angle between the positron momentum vector in the J/ψ rest frame and the J/ψ momentum vector in the laboratory frame. The full angular distribution, which is derived from the density matrix elements of the production amplitude using parity conservation rules, is described

by:

$$\frac{d^2N}{d(\cos\theta)d\phi} \propto 1+\lambda_\theta \cos^2\theta+\lambda_\phi \sin^2\theta\cos 2\phi+\lambda_{\theta\phi}\sin 2\theta\cos\phi\,, \tag{1}$$

where θ and ϕ are polar and azimuthal angles, respectively; λ_θ and λ_ϕ are the angular decay coefficients. The angular distribution integrated over the azimuthal angle is parametrized as

$$\frac{dN}{d(\cos\theta)} \propto 1+\lambda_\theta\cos^2\theta\,, \tag{2}$$

where λ_θ is called the polarization parameter. This parameter contains both the longitudinal and transverse components of the J/ψ cross section; $\lambda_\theta = 1$ indicates full transverse polarization, and $\lambda_\theta = -1$ corresponds to full longitudinal polarization.

The measurement presented in this Letter is limited to the θ angle analysis due to statistical limitations. Extraction of the λ_θ parameter in the helicity frame allows one to compare the result with the available model predictions and draw model dependent conclusions. A measurement of the θ angle with a better precision, as well as the ϕ angle, will be possible with a newer STAR data at $\sqrt{s} = 500$ GeV. Then, the frame invariant parameter, also in different reference frames, can be calculated providing model independent information about the J/ψ polarization [31].

II. DATA ANALYSIS

A. Data set and electron identification

The $p+p$ 200 GeV data used in this analysis were recorded by the STAR experiment in the year 2009. The STAR detector [32] is a multi-purpose detector. It consists of many subsystems and has cylindrical geometry and a large acceptance with a full azimuthal coverage. The most important subsystems for this analysis are briefly described below. The Time Projection Chamber (TPC) [33] is the main tracking detector for charged particles. It is also used to identify particles using the ionization energy loss (dE/dx). Outside the TPC is the Time Of Flight (TOF) detector [34] which extends STAR particle identification capabilities to momentum ranges where TPC dE/dx alone is inadequate. Between the TOF and the STAR magnet there is the STAR Barrel Electromagnetic Calorimeter (BEMC) [35]. The BEMC is constructed so that an electron should deposit all its energy in the BEMC towers while hadrons usually deposit only a fraction of their energy. The energy deposited by a particle in the BEMC can thus be used to discriminate between electrons and hadrons, by looking at the E/p ratio. The BEMC is also used to trigger on high-p_T electrons. Together with the TOF, the BEMC is utilized to discriminate against pile-up tracks in the TPC, since both detectors are fast. Most of the STAR detector subsystems are enclosed in a room temperature solenoid magnet with a uniform magnetic field of maximum value of 0.5 T [36].

The analyzed data were collected with the High Tower (HT) trigger, which requires transverse energy deposited in at least one single tower of the BEMC to be within $2.6 < E_T \leq 4.3$ GeV. The HT trigger also requires a coincidence signal from two Vertex Position Detectors [37]. We have analyzed $\sim$ 33 M events with the HT trigger and with a primary vertex z position $|V_z| < 65$ cm. This corresponds to an integrated luminosity of $\sim$ 1.6 pb^{-1}. The J/ψ is reconstructed via its di-electron decay channel, $J/\psi \to e^+e^-$, with the branching ratio $5.94\% \pm 0.06\%$ [38].

Charged tracks are reconstructed using the STAR TPC which has 2π azimuthal coverage and a pseudorapidity (η) coverage of $|\eta| < 1$. Tracks that originate from the primary vertex and have a distance of closest approach (DCA) to the primary vertex of less than 2 cm are used. In 2009 STAR did not have a vertex detector that would help to distinguish between prompt and non-prompt J/ψ, and TPC resolution alone is not enough to select non-prompt J/ψ from B meson decays. In order to ensure a good track quality, tracks are required to have at least 15 points used in the track reconstruction in the TPC, and to have at least 52% of the maximum number of possible track reconstruction points. Cuts of $|\eta| < 1$ and $p_T > 0.4$ GeV/c are also applied. The transverse momentum cut is chosen to optimize the acceptance in $\cos\theta$ and the significance of the J/ψ signal. Applying higher p_T cut causes a loss of statistics at $|\cos\theta| \sim 1$ while a lower p_T cut reduces the J/ψ signal significance. Efficient identification of electrons with low p_T was possible using available information from the TOF detector. During the analyzed run in 2009, 72% of the full TOF detector was installed. The TOF pseudorapidity coverage is $|\eta| < 0.9$.

In order to identify electrons and reject hadrons, information from the TPC, TOF and BEMC detectors is used. The TPC provides information about dE/dx of a particle in the detector. Electron candidates are required to have $n\sigma_{\rm electron}$ within $-1 < n\sigma_{\rm electron} < 2$, where $n\sigma_{\rm electron} = \log[(dE/dx)/(dE/dx\mid_{\rm Bichsel})]/\sigma_{dE/dx}$, dE/dx is the measured energy loss in the TPC, $dE/dx\mid_{\rm Bichsel}$ is the expected value of dE/dx from the Bichsel function prediction [39] and $\sigma_{dE/dx}$ is the dE/dx resolution. The Bichsel function is used to calculate the energy dependence of the most probable energy loss of the ionization spectrum from a detector. In a thin material such as the TPC gas, it has been shown that the Bichsel function is a very good approximation for the dE/dx curves [40]. At lower momenta (p $\lesssim$ 1.5 GeV/c), where electron and hadron dE/dx bands overlap, the TOF detector is used to reject slow hadrons. For $p < 1.4$ GeV/c, a cut on the speed of a particle, β, of $|1/\beta - 1| < 0.03$ is applied. At higher momenta, the BEMC rejects hadrons efficiently. For momenta above 1.4 GeV/c, a cut on $E/p > 0.5$ c is used for electron identification, where E is the energy de-

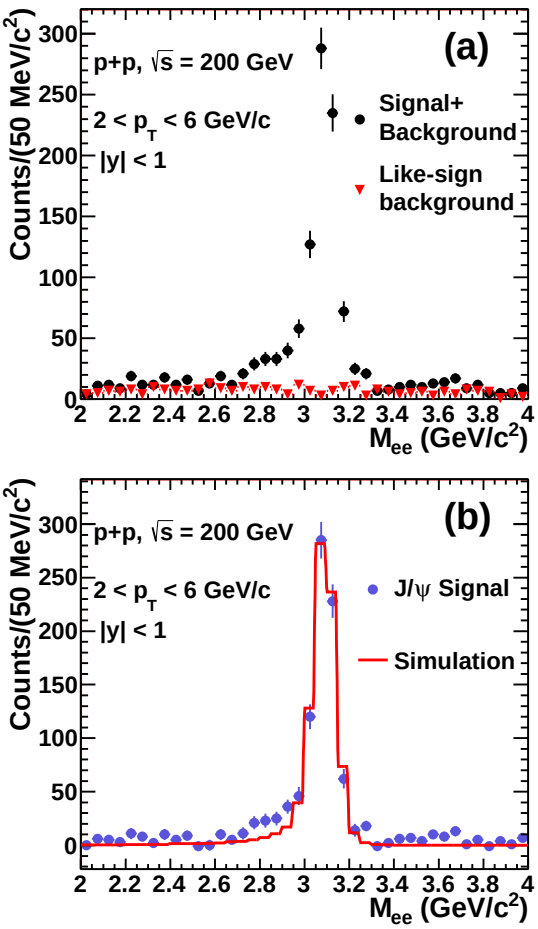

FIG. 1: (Color online.) (a) Invariant mass distributions of unlike-sign (black circles) and like-sign (red triangles) electron/positron pairs, for $2 < p_T < 6$ GeV/c and $|y| < 1$. (b) J/ψ signal after the combinatorial background subtraction (closed blue circles) and MC simulation (histogram).

posited in a single BEMC tower ($\Delta\eta \times \Delta\phi = 0.05 \times 0.05$). For electrons, the ratio of total energy deposited in the BEMC to the particle's momentum is expected to be ≈ 1. In the analysis we use energy deposited in a single BEMC tower but an electron can deposit its energy in more towers, therefore the value of the E/p cut is 0.5 c.

It is also required that at least one of the electrons from the J/ψ decay satisfies the HT trigger conditions. In order to ensure that a selected electron indeed fired the trigger, an additional cut of $p_T > 2.5$ GeV/c is applied for that electron. The HT trigger requirements reduce significantly the combinatorial background under the J/ψ signal and lead to a clear J/ψ signal at $2 < p_T < 6$ GeV/c.

B. J/ψ signal and $\cos\theta$ distributions

Electrons and positrons that pass track quality and electron identification (eID) cuts are paired in each event. Figure 1(a) shows the invariant mass distribution for dielectron pairs with $|y| < 1$ and p_T of 2 - 6 GeV/c. The unlike-sign pairs are represented by circles. The combinatorial background is estimated using the like-sign technique, and is defined as a sum of all e^+e^+ and e^-e^- pairs in an event, represented by triangles. The J/ψ signal is obtained by subtracting the combinatorial background from the unlike-sign pair distribution. Figure 1(b) shows the invariant mass distribution for J/ψ as circles, and the histogram is the J/ψ signal obtained from a Monte Carlo (MC) simulation (see Sec. II C). Momentum resolution of electrons and positrons from the MC simulation is additionally smeared in order that the simulated J/ψ signal width matches the width of the J/ψ signal obtained from the data. The simulation does not include the J/ψ radiative decay channel, $J/\psi \to e^+e^-\gamma$ [11, 38], leading to the discrepancy between data and simulation for invariant mass $\sim$ 2.7 - 2.9 GeV/c^2. The tail in the data at low invariant mass is due to electron bremsstrahlung and missing photons in the case of the J/ψ radiative decay reconstruction. We select J/ψ candidates in the invariant mass range 2.9 - 3.3 GeV/c^2 and so the discrepancy between the data and the simulation for the lower mass range does not influence our result.

In the analyzed ranges of rapidity, p_T, and invariant mass, the signal to background ratio is 15. A strong J/ψ signal is seen with a significance of 26 σ. The number of J/ψ, obtained by counting data entries in the J/ψ mass window, is 791 $\pm$ 30. For the polarization analysis, we split the entire J/ψ sample into 3 p_T bins with a comparable number of J/ψ in each bin: 2 - 3 GeV/c, 3 - 4 GeV/c and 4 - 6 GeV/c.

Raw $\cos\theta$ distributions for J/ψ (after the combinatorial background subtraction) are obtained by bin counting, using distributions from the data. Figures 2(a)-(c) show uncorrected $\cos\theta$ distributions (full squares).

C. Corrections

In order to obtain the $\cos\theta$ corrections, unpolarized Monte Carlo J/ψ particles with uniform p_T and rapidity distributions are embedded into real events, and the STAR detector response is simulated. Since the input p_T and rapidity shapes influence efficiencies, J/ψ distributions are then weighted according to the J/ψ p_T and rapidity shapes observed in the STAR [11] and PHENIX [41] experiments. Corrected $\cos\theta$ distributions are obtained by dividing raw $\cos\theta$ distributions by the corrections calculated as a function of $\cos\theta$, in each analyzed p_T bin.

Efficiencies as a function of $\cos\theta$ are calculated by applying the same cuts used in the data analysis to the embedding (simulation) sample. Most corrections related to the TPC response, such as the acceptance (with the p_T and η cuts) and tracking efficiency, and all BEMC efficiencies, are obtained from the simulation. The $n\sigma_{\rm electron}$ and the TOF response are not simulated accurately in

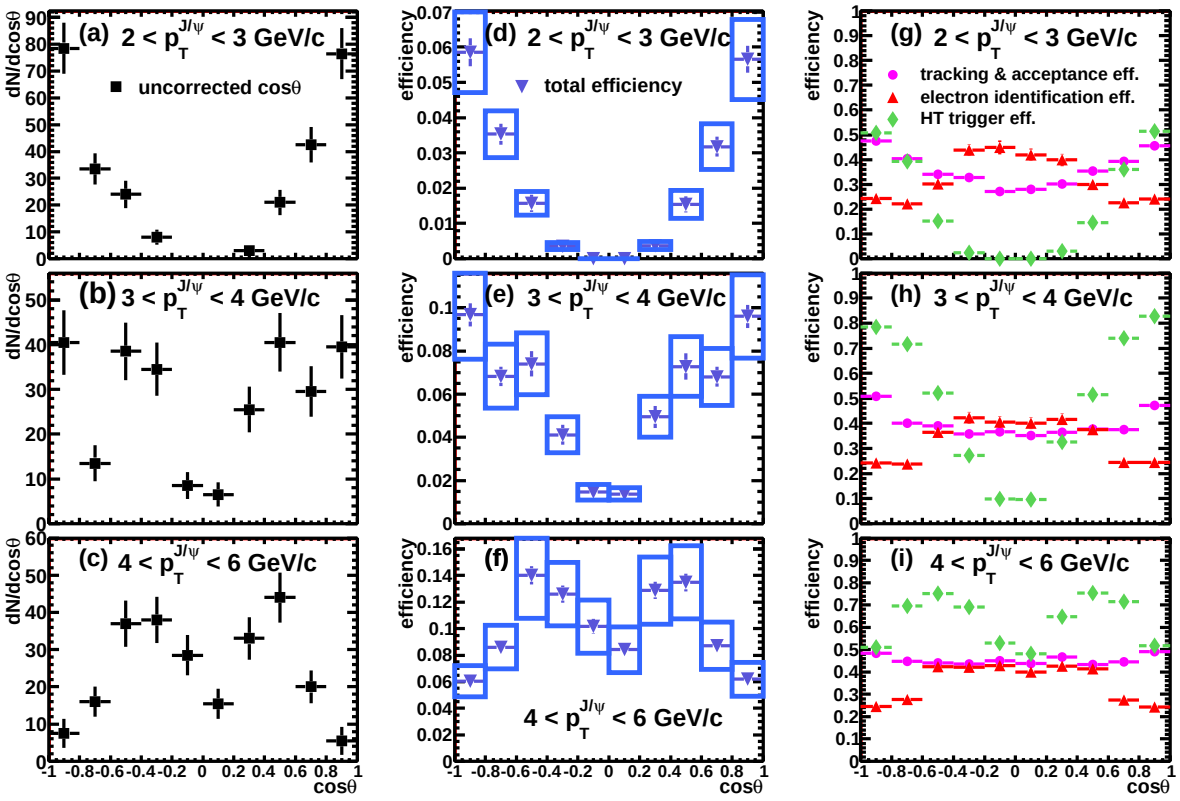

FIG. 2: (Color online.) Panels (a)-(c) show uncorrected $\cos\theta$ distributions after the combinatorial background subtraction, for each analyzed p_T bin. Panels (d)-(f) show total efficiencies as a function of $\cos\theta$. Systematic errors are shown as boxes. Panels (g)-(i) show different efficiencies that contribute to the total efficiency.

embedding. Therefore the $n\sigma_{\rm electron}$ cut and TOF cut efficiencies are calculated using the data.

For the calculation of the $n\sigma_{\rm electron}$ cut efficiency, the $n\sigma_{\rm electron}$ distribution from the data is approximated with a sum of Gaussian functions (one Gaussian function for electrons and two Gaussian functions for hadrons), in narrow momentum bins. In order to improve the fitting, the TOF and BEMC eID cuts are applied and the position of the Gaussian fit for electrons is constrained using a high-purity (almost 100%) electron sample obtained by selecting photonic electrons and subtracting a background from like-sign electron pairs. Photonic electrons are produced from photon conversion in the detector material and Dalitz decay of π^0 and η mesons. These electrons are isolated using a cut on the invariant mass of a pair of tracks of $m_{e^-e^+} < 100$ MeV/c^2 and additional electron identification cuts: $|1/\beta - 1| < 0.03$ for $p < 1.5$ GeV/c and $E/p > 0.5$ c for momenta above 1.5 GeV/c.

TOF matching efficiency is calculated using a low luminosity data sample (with almost no pile-up). Since the TOF detector did not have full coverage in 2009, the TOF matching efficiency is applied in the total efficiency calculation as a function of η. The efficiency of the $1/\beta$ cut is calculated by using a pure electron sample obtained by selecting photonic electrons with $-0.2 < n\sigma_e < 2$ and with the invariant mass of a pair of tracks less than 15 MeV/c^2. The $1/\beta$ cut efficiency is calculated in narrow momentum bins and then a constant function is fitted to obtain the final $1/\beta$ cut efficiency.

The total J/ψ efficiency calculations include contributions from the acceptance, the tracking efficiency, the electron identification efficiency, and the HT trigger efficiency, and are shown as a function of $\cos\theta$ in Fig. 2(d)-(f) (blue triangles). The systematic uncertainties (discussed in subsection III B) on the total efficiency are also shown in the figure. The right-hand panels, Fig. 2(g)-(i), show separately the efficiencies that contribute to the total efficiency.

The most important factor influencing the shape of the total efficiency is the HT trigger efficiency, which is shown as green diamonds in Fig. 2(g)-(i). At least one of the electrons from the J/ψ decay is required to satisfy the trigger conditions and must have p_T above 2.5 GeV/c. Due to the decay kinematics this cut causes significant loss in the number of observed J/ψ at lower J/ψ p_T, and the efficiency decreases with decreasing $|\cos\theta|$. This pattern is clearly visible in the HT trigger efficiency plot for $2 < p_T < 3$ GeV/c in Fig. 2(g), where all entries at $\cos\theta \sim 0$ are zero. With increasing J/ψ p_T, the trigger efficiency increases. Since the trigger has also an upper threshold ($E_T \leq 4.3$ GeV), a decrease of the efficiency at $|\cos\theta| \sim 1$ at higher p_T is seen, as evident in Fig. 2(i).

III. RESULTS AND DISCUSSION

A. Corrected $\cos\theta$ distributions

The corrected $\cos\theta$ distributions are fitted with

$$f(\cos\theta) = C(1 + \lambda_\theta \cos^2\theta) \quad (3)$$

where C is a normalization factor and λ_θ is the polarization parameter. The fitting procedure is carried out with no constraints applied to the fit parameters. The corrected $\cos\theta$ distributions with the fits are shown in Fig. 3. The errors shown are statistical only. The solid line represents the most likely fit. The band around the line is a 1σ uncertainty contour on the fit, which takes into account uncertainties on both fit parameters and correlations between them. The measured values of the polarization parameter, in each analyzed p_T bin, are listed in Table I together with a mean p_T ($\langle p_T \rangle$) in each bin and statistical and systematic uncertainties.

p_T (GeV/c)	$\langle p_T \rangle$ (GeV/c)	λ_θ
$2 < p_T < 3$	2.48	0.15 ± 0.33 (stat.) ± 0.30 (sys.)
$3 < p_T < 4$	3.52	-0.48 ± 0.16 (stat.) ± 0.16 (sys.)
$4 < p_T < 6$	4.74	-0.62 ± 0.18 (stat.) ± 0.26 (sys.)

TABLE I: The polarization parameter λ_θ.

B. Systematic uncertainties

The systematic uncertainties on the polarization parameter λ_θ are summarized in Table II. All sources, except the last two, contribute to the error on the total efficiency and are included in the systematic uncertainties shown in Fig. 2(d)-(f). Each contribution is described below. Each systematic uncertainty is the maximum deviation from the central value of λ_θ. The systematic uncertainties are combined assuming that they are uncorrelated, and are added in quadrature.

Tracking efficiency

The systematic uncertainty on the tracking efficiency arises from small differences between the simulation of the TPC response in the embedding calculation and the data. Track properties, DCA and the number of points used in the track reconstruction in the TPC (fitPts), are compared between simulation and data. The systematic uncertainty is due to a shift of the fitPts distribution (by 2 points) in the simulation. The uncertainty is considered symmetric.

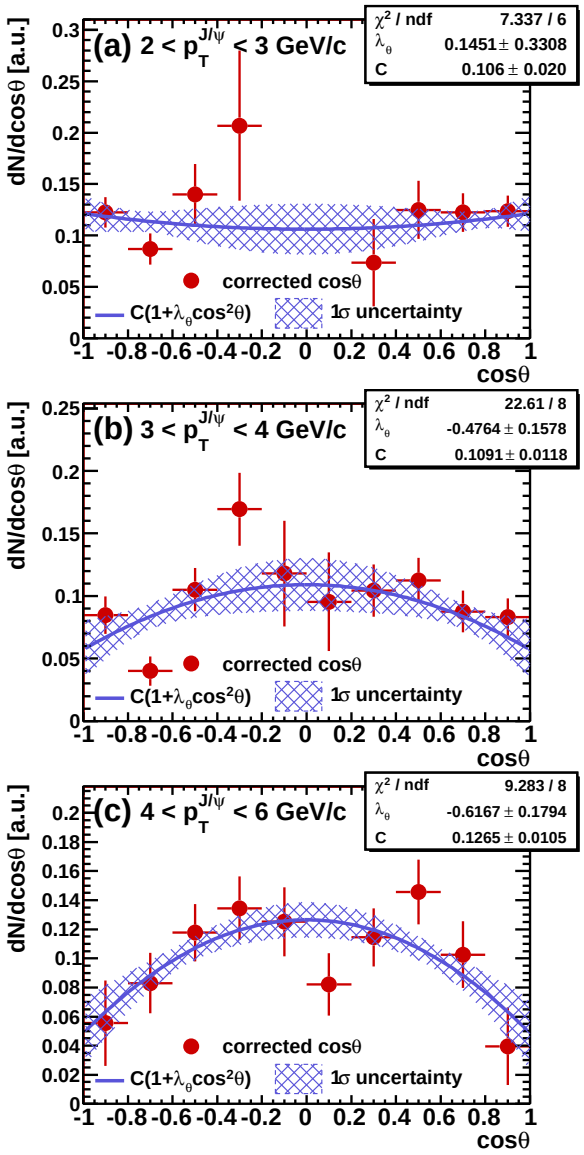

FIG. 3: (Color online.) Corrected $\cos\theta$ distributions fitted with the function in Eq. 3. The plotted errors are statistical. The solid blue lines represent the most likely fits, and the hatched blue bands represent the 1σ uncertainty on the fits.

TPC eID efficiency

The systematic uncertainty from TPC electron identification is estimated by changing constraints on the mean and width of the Gaussian fit for electrons and recalculating the total efficiency. The constraints put on the mean and width are allowed to vary by 3σ.

TOF efficiency

Since the TOF detector did not have full coverage in 2009, the TOF matching efficiency is applied in the total efficiency calculation as a function of η. The system-

atic uncertainty is estimated with the TOF matching efficiency also being a function of azimuthal angle ϕ. The $1/\beta$ cut efficiency estimated from the data in small p_T bins may be sensitive to fluctuations. The $1/\beta$ distribution obtained from the data is well described by the Gaussian function. So the systematic uncertainty on the $1/\beta$ cut efficiency is estimated by applying the efficiency calculated for the whole momentum range of $0.4 < p < 1.4$ GeV/c from a Gaussian fit to the $1/\beta$ distribution.

BEMC efficiency

Differences between the simulated BEMC response and the BEMC response in the real data may affect the matching of a TPC track to the BEMC detector and the efficiency of the E/p cut. The matching efficiency of a TPC track to the BEMC and the E/p distribution are compared between data and simulation. A pure electron sample from the data is obtained by selecting photonic electrons with $-0.2 < n\sigma_e < 2$ and with the invariant mass of a pair of tracks less than 15 MeV/c^2. The systematic uncertainty of the BEMC efficiency is estimated by applying BEMC matching and E/p cut efficiencies obtained from the data instead of using simulated BEMC response, in the total efficiency calculation.

HT trigger efficiency

HT trigger response in the simulation, energy in a BEMC tower, is compared with the BEMC response in the data. The systematic uncertainty on the HT trigger efficiency is estimated by varying the trigger turn-on conditions in the simulation by the difference seen between data and simulation, which is 3%.

Input J/ψ distribution in the simulation

Since the input J/ψ transverse momentum and rapidity distributions in the simulation are flat, they need to be weighted with realistic p_T and rapidity spectra. In order to estimate a systematic uncertainty, the p_T and rapidity weights are changed. The p_T weight is varied by changing the ranges in which the Kaplan [42] function is fitted to the p_T spectrum. The weight used for rapidity is obtained by fitting a Gaussian function to the rapidity spectrum, and the systematic uncertainty is estimated by assuming that the rapidity shape is flat at mid-rapidity.

Also, the J/ψ particles in the simulation are unpolarized (the input $\cos\theta$ distribution is flat). The acceptance of electron and positron from the J/ψ decay in the detector depends on the J/ψ polarization. In order to estimate the effect of the unknown J/ψ polarization on the acceptance calculation, fully transverse ($\lambda_\theta = 1$) and fully longitudinal ($\lambda_\theta = -1$) J/ψ polarization is assumed in the embedding analysis. A systematic uncertainty is estimated as a difference between the result obtained with no input J/ψ polarization and the result when J/ψ in the simulation is polarized. An average uncertainty from the two input J/ψ polarizations, longitudinal and transverse, is taken as a systematic uncertainty in this study.

	Systematic uncertainty on λ_θ, in p_T (GeV/c) bins		
Source	2 - 3	3 - 4	4 - 6
Tracking efficiency	0.024	0.009	0.008
TPC eID efficiency	0.009	0.006	0.012
TOF efficiency	0.057	0.018	0.014
BEMC efficiency	0.035	0.024	0.068
HT trigger efficiency	0.049	0.006	0.003
Input J/ψ distributions in the simulation	0.190	0.019	0.027
Errors from the simulation	0.077	0.028	0.004
Polarization of the continuum background	0.025	0.034	0.034
J/ψ signal extraction	0.195	0.149	0.246
Total	$\pm$0.297	$\pm$0.160	$\pm$0.260

TABLE II: Systematic uncertainties.

Errors from the simulation

Statistical errors on the total efficiencies, determined using the MC simulation, are included in the systematic uncertainties.

Polarization of the continuum background

In Fig. 1(b), it is seen that there is still some residual continuum background after the combinatorial background subtraction. This background consists of correlated $c\overline{c} \to e^+e^-$ and $b\overline{b} \to e^+e^-$. The continuum background is about 5 % of the measured J/ψ in the analyzed invariant mass range. Due to the small statistics of the continuum background, we are not able to estimate a polarization of the correlated background using our data. Instead, we use the value obtained by the PHENIX experiment [27]. They found that the continuum polarization is between -0.3 and 0.3. We estimate a systematic uncertainty by simulating $\cos\theta$ distributions for the residual background taking two extreme values of λ_θ: -0.3 and 0.3. Then those $\cos\theta$ distributions are subtracted from the corrected $\cos\theta$ distributions from the data, assuming that the residual background is 5% of the J/ψ yield, in order to estimate the influence of the continuum background polarization on the measured λ_θ.

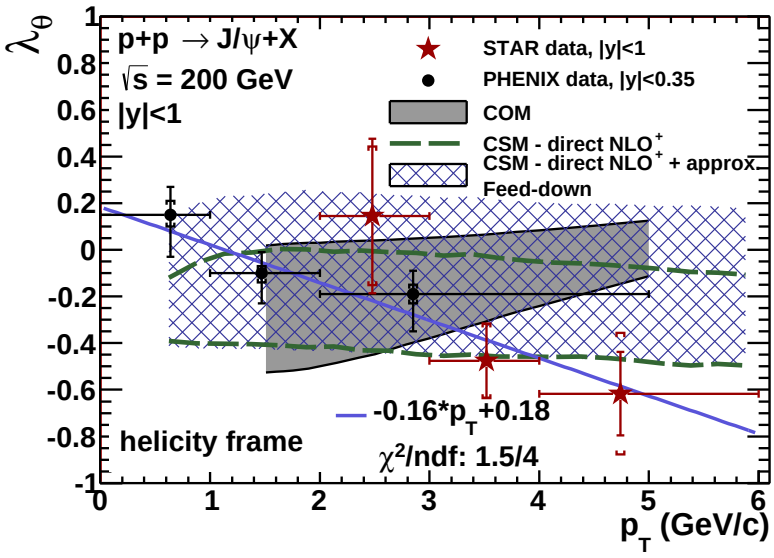

FIG. 4: (Color online.) Polarization parameter λ_θ as a function of J/ψ p_T (red stars) for $|y| < 1$. The data is compared with the PHENIX result (black solid circles) [27] and two model predictions: NLO$^+$ Color Singlet Model (CSM) (green dashed lines represent a range of λ_θ for the direct J/ψ , and the hatched blue band is an extrapolation of λ_θ for the prompt J/ψ) [28] and LO NRQCD calculations with color-octet contributions (COM) [26] (gray shaded area). The p_T coverages of the CSM and COM models are $\sim$ 0.6 - 6.0 GeV/c and $\sim$ 1.5 - 5.0 GeV/c, respectively. The horizontal error bars represent widths of p_T bins. The blue line is a linear fit ($Ax + B$) to RHIC points.

J/ψ signal extraction

The systematic uncertainty associated with the J/ψ signal extraction is estimated by counting the number of J/ψ particles using the simulated J/ψ signal shape. The J/ψ signal from the simulation is extracted in each p_T and $\cos\theta$ bin and fitted to the data.

C. Polarization parameter λ_θ

Figure 4 shows the polarization parameter λ_θ as a function of J/ψ p_T for inclusive J/ψ production. The result includes direct J/ψ production, as well as J/ψ from feed-down from heavier charmonium states, $\psi^{'}$ and χ_C (about 40% of the prompt J/ψ yield [43]), as well as from B meson decays (non-prompt J/ψ) [11]. The non-direct J/ψ production may influence the observed polarization. The STAR result (red stars) is compared with the PHENIX mid-rapidity ($|y| < 0.35$) J/ψ polarization result for inclusive J/ψ [27] (black solid circles). The blue line is a linear fit, which takes into account both statistical and systematic uncertainties, to all RHIC points. The fit gives a negative slope parameter -0.16 ± 0.07 with χ^2/ndf = 1.5/4. A trend towards longitudinal J/ψ polarization is seen in the RHIC data.

STAR observes longitudinal J/ψ polarization in the helicity frame at $p_T > 3$ GeV/c. The STAR and PHENIX measurements are consistent with each other in the overlapping p_T region. Our result can be compared to the polarization measurements from CDF [20] and CMS [22] at mid-rapidity for prompt J/ψ. At $p_T \sim 5$ GeV/c, CDF observes almost no polarization, $\lambda_\theta \sim 0$ (the polarization becomes slightly longitudinal as p_T increases) while STAR observes a strong longitudinal polarization in that p_T region. At LHC $\sqrt{s} = 7$ TeV, CMS reports zero polarization at mid-rapidity up to $p_T \sim 70$ GeV/c [22]. In addition, the ALICE experiment also reports very small polarization within $2 < p_T < 8$ GeV/c at forward rapidity [24]. However, if the J/ψ production is x_T dependent [10], the RHIC result at $p_T \sim 2$ GeV/c is comparable with the CDF result at $p_T \sim 20$ GeV/c and with the CMS result at $p_T \sim 70$ GeV/c ($x_T \sim 0.02$, $x_T = 2p_T/\sqrt{s}$).

The data are compared with two model predictions for λ_θ at mid-rapidity: NLO$^+$ CSM [28] and LO COM [26]. The prediction of the COM [26] for direct J/ψ production, the gray shaded area, moves towards the transverse J/ψ polarization as p_T increases [20]. The trend seen in the STAR and PHENIX results is towards longitudinal J/ψ polarization with increasing p_T, and a linear fit to the RHIC data has a negative slope parameter. The difference between the central value of the COM model calculations and the STAR data in terms of χ^2/ndf (P value) is 6.7/3 (8.2×10^{-2}). The COM failed to describe the polarization measurements by the CDF and CMS experiments at higher energies.

Green dashed lines represent a range of λ_θ for the direct J/ψ production from the NLO$^+$ CSM prediction and an extrapolation of λ_θ for the prompt J/ψ production is shown as the hatched blue band [28]. It predicts a weak p_T dependence of λ_θ, and within the experimental and theoretical uncertainties, the RHIC result is consis-

tent with the NLO$^+$ CSM model prediction. Comparison between the central value of the NLO$^+$ CSM prediction and the STAR data gives χ^2/ndf (P value) of 3.0/3 (3.9×10^{-1}) and 5.1/3 (1.6×10^{-1}) for the direct and prompt J/ψ production, respectively.

IV. SUMMARY AND OUTLOOK

This paper reports the first STAR measurement of J/ψ polarization and contributes to the evolving understanding of the J/ψ production mechanisms. J/ψ polarization is measured in $p+p$ collisions at $\sqrt{s} = 200$ GeV in the helicity frame at $|y| < 1$ and $2 < p_T < 6$ GeV/c. RHIC data indicates a trend towards longitudinal J/ψ polarization as p_T increases. The result is consistent, within experimental and theoretical uncertainties, with the NLO$^+$ CSM model.

Newer data at $\sqrt{s} = 500$ GeV, taken in 2011 with much higher luminosity, may help to further distinguish between J/ψ production models, and may permit analysis of the full angular distribution. Furthermore, uncertainties in the models need to be reduced in order to draw more precise conclusions from experimental measurements.

Acknowledgements

We thank the RHIC Operations Group and RCF at BNL, the NERSC Center at LBNL, the KISTI Center in Korea and the Open Science Grid consortium for providing resources and support. This work was supported in part by the Offices of NP and HEP within the U.S. DOE Office of Science, the U.S. NSF, CNRS/IN2P3, FAPESP CNPq of Brazil, Ministry of Ed. and Sci. of the Russian Federation, NNSFC, CAS, MoST and MoE of China, the Korean Research Foundation, GA and MSMT of the Czech Republic, FIAS of Germany, DAE, DST, and CSIR of India, National Science Centre of Poland, National Research Foundation (NRF-2012004024), Ministry of Sci., Ed. and Sports of the Rep. of Croatia, and RosAtom of Russia.

[1] M. Einhorn, S. Ellis, Phys.Rev. D12 (1975) 2007.
[2] S. Ellis, M. B. Einhorn, C. Quigg, Phys.Rev.Lett. 36 (1976) 1263.
[3] C. Carlson, R. Suaya, Phys.Rev. D14 (1976) 3115.
[4] C. Chang, Nucl.Phys. B172 (1980) 425–434.
[5] E. L. Berger, D. L. Jones, Phys.Rev. D23 (1981) 1521–1530.
[6] R. Baier, R. Ruckl, Phys.Lett. B102 (1981) 364.
[7] R. Baier, R. Ruckl, Nucl.Phys. B201 (1982) 1.
[8] R. Baier, R. Ruckl, Z.Phys. C19 (1983) 251.
[9] E. Braaten, S. Fleming, T. C. Yuan, Ann. Rev. Nucl. Part. Sci. 46 (1996) 197–235.
[10] B. Abelev, *et al.* (STAR Collaboration), Phys. Rev. C 80 (2009) 041902.
[11] L. Adamczyk, *et al.* (STAR Collaboration), Phys. Lett. B 722 (2013) 55–62.
[12] A. Adare, *et al.* (PHENIX Collaboration), Phys.Rev. D85 (2012) 092004.
[13] F. Abe, *et al.* (CDF Collaboration), Phys. Rev. Lett. 79 (1997) 572–577.
[14] D. Acosta, *et al.* (CDF Collaboration), Phys.Rev. D71 (2005) 032001.
[15] G. Aad, *et al.* (ATLAS Collaboration), Nucl.Phys. B850 (2011) 387–444.
[16] V. Khachatryan, *et al.* (CMS Collaboration), Eur.Phys.J. C71 (2011) 1575.
[17] R. Aaij, *et al.* (LHCb Collaboration), Eur.Phys.J. C71 (2011) 1645.
[18] E. Braaten, B. A. Kniehl, J. Lee, Phys. Rev. D 62 (2000) 094005.
[19] M. Butenschoen, B. A. Kniehl, Nucl.Phys.Proc.Suppl. 222-224 (2012) 151–161.
[20] A. Abulencia, *et al.* (CDF Collaboration), Phys. Rev. Lett. 99 (2007) 132001.
[21] M. Butenschoen, B. A. Kniehl, Phys.Rev.Lett. 108 (2012) 172002.
[22] S. Chatrchyan, *et al.* (CMS Collaboration), arXiv:1307.6070 (2013).
[23] B. Gong, L.-P. Wan, J.-X. Wang, H.-F. Zhang, Phys.Rev.Lett. 110 (2013) 042002.
[24] B. Abelev, *et al.* (ALICE Collaboration), Phys.Rev.Lett. 108 (2012) 082001.
[25] R. Aaij, *et al.* (LHCb Collaboration), Eur.Phys.J. C73 (2013) 2631.
[26] H. S. Chung, C. Yu, S. Kim, J. Lee, Phys. Rev. D 81 (2010) 014020.
[27] A. Adare, *et al.* (PHENIX Collaboration), Phys. Rev. D 82 (2010) 012001.
[28] J. Lansberg, Phys. Lett. B 695 (2011) 149–156, and private communication (2013).
[29] J. Lansberg, J.Phys. G38 (2011) 124110.
[30] C. S. Lam, W.-K. Tung, Phys. Rev. D 18 (1978) 2447–2461.
[31] P. Faccioli, C. Lourenco, J. Seixas, H. K. Wohri, Eur. Phys. J. C 69 (2010) 657–673.
[32] K. Ackermann, *et al.* (STAR Collaboration), Nucl. Instrum. Meth. A 499 (2003) 624–632.
[33] M. Anderson, *et al.*, Nucl. Instrum. Meth. A 499 (2003) 659–678.
[34] W. J. Llope, *et al.*, Nucl. Instrum. Meth. A 661 (2012) 110–113.
[35] M. Beddo, *et al.* (STAR Collaboration), Nucl. Instrum. Meth. A 499 (2003) 725–739.
[36] F. Bergsma, *et al.*, Nucl. Instrum. Meth. A 499 (2003) 633–639.
[37] W. J. Llope, *et al.*, Nucl. Instrum. Meth. A 522 (2004) 252–273.
[38] J. Beringer, *et al.* (Particle Data Group), Phys. Rev. D 86 (2012) 010001, the branching ratio for $J/\psi \to e^+e^-$ is (5.94 ± 0.06)%, including (0.88 ± 0.14)% for $J/\psi \to$

$e^+e^-\gamma$.
[39] H. Bichsel, STAR Note SN0439 (2001).
[40] H. Bichsel, Nucl.Instrum.Meth. A562 (2006) 154–197.
[41] A. Adare, *et al.* (PHENIX Collaboration), Phys. Rev. Lett. 98 (2007) 232002.
[42] D. Kaplan, *et al.*, Phys. Rev. Lett. 40 (1978) 435–438.
[43] S. J. Brodsky, J.-P. Lansberg, Phys. Rev. D 81 (2010) 051502.